Surface morphology of tungsten exposed to helium plasma at temperatures below fuzz formation threshold 1073 K

メタデータ	言語: English 出版者: 公開日: 2021-12-15 キーワード (Ja): キーワード (En): 作成者: SAKAMOTO, Ryuichi, Bernard, Elodie, Kreter, Arkadi, YOSHIDA, Naoaki メールアドレス: 所属:
URL	http://hdl.handle.net/10655/00012712

This work is licensed under a Creative Commons Attribution-NonCommercial-ShareAlike 3.0 International License.

Surface Morphology of Tungsten Exposed to Helium Plasma at Temperatures below Fuzz Formation Threshold 1073 K

Ryuichi Sakamoto[1,5], Elodie Bernard[2], Arkadi Kreter[3] and Naoaki Yoshida[4]

[1] National Institute for Fusion Science, Toki, Gifu 509-5292, Japan

[2] Aix-Marseille University, Marseille, 13288, France

[3] Forschungszentrum Jülich GmbH, Institut für Energie- und Klimaforschung - Plasmaphysik, 52425 Jülich, Germany

[4] Kyushu University, Kasuga, Fukuoka 816-8580, Japan

[5] The Graduate University for Advanced Studies, Toki, Gifu 509-5292, Japan

E-mail: `sakamoto@nifs.ac.jp`

Abstract. An impact of crystal orientation on the surface morphology of the helium plasma exposed tungsten has been investigated on the linear device PSI-2. A nanoscale undulating surface structure which has a periodic arrangement is formed for temperatures below 1073 K, in contrast to the fuzz nanostructure formation in a higher temperature range. The crests of undulation align with the <100> direction. The interval of the undulation is the narrowest at the crystal grain of {110} surface. The interval becomes wider as the crystal grain surface is tilting away from the {110} surface, and the undulating surface structure is not formed near the {100} surface. The height of undulations is ~ 8 nm independently of the interval of the undulations, and it corresponds to a depth of the layer heavily damaged sue to helium plasma exposure.

PACS numbers: 61.05.J-, 68.37.Hk, 68.37.Lp, 68.47.De

Submitted to: *Nuclear Fusion*

1. Introduction

Tungsten is a prime candidate for the plasma facing material in a fusion reactor due to its excellent high temperature properties, high sputtering threshold energy, low hydrogen retention and acceptable induced radioactivity [1]. In the fusion reactor, the plasma facing materials are exposed not only to hydrogen isotope fuel but also to helium ash, which is generated by fusion reactions. At the first wall, the total incident particle flux is estimated as $10^{21} - 10^{22}$ particles/m^{2}s, and several % of helium particles will be included in the incident flux. There are many experiments which indicate the strong effect of the helium irradiation on the surface morphology of tungsten even in the range of low energy below a threshold of the displacement damage, e.g., nano bubble, hole and fuzz nanostructure [2–5]. Furthermore, previous investigations have shown that hydrogen isotope retention is significantly affected by helium distribution in the tungsten surface layer [6, 7]. These results emphasize the importance of helium effects on tungsten as a plasma facing material.

Plasma confinement devices of the present day are equipped with a sufficiently thick and solid first wall to protect the vacuum vessel from the incident heat and particles originating from scrape-off-layer plasma and charge exchange particles [8–11]. In the fusion reactor, a blanket, whose function will also be to breed tritium fuel, must be installed facing the plasma. In order to obtain a reasonable tritium breeding ratio, minimization of the neutron attenuation is required at the blanket surface, and, therefore, thick protection will not be allowed at the first wall. Only a thin tungsten coating layer (sub mm to few mm) is envisaged as the first wall to protect the blanket from the incident heat and particles in spite of harsher conditions than in current devices [12, 13]. The first wall temperature, i.e., the blanket surface temperature, must be kept at the allowable maximum temperature of structural material of the blanket for high-efficiency power generation. The maximum temperature is $\sim$ 823 K in the case of the RAFS (Reduced-Activation Ferritic/Martensitic Steels) [14] and $\sim$ 973 K in the case of the vanadium alloy [15]. The operational temperature of the the first wall must be, therefore, significantly below 900 °C, which is the lower threshold temperature of the fuzz nanostructure formation [3]. Although a large number of studies have been published on the fuzz nano structure, little attention has been paid to temperature ranges below the threshold temperature.

We conducted the helium plasma exposure experiments using the Large Helical Device (LHD) at the same temperature as the first wall of the fusion reactor. The

experimental results show that a heavily damaged layer is formed at the very surface layer. Nano-bubbles are observed much deeper than the range of helium implantation raising concerns about the consequences for the material properties conservation [16]. According to nano-indentation measurements, the hardness of exposed tungsten indeed increases as the dislocation loops are tangled up and large bubbles appear in the material. In these experiments, however, the flux and fluence were rather low to predict the material damages at the first wall in the fusion reactor. In order to explore the helium effects on tungsten under the higher flux and fluence conditions, helium plasma exposure experiments have been carried out in linear plasma device PSI-2 [17].

In this paper, we will describe helium effects on tungsten at the operating temperature of the fusion reactor from the view point of surface morphology.

2. Experimental

The samples were high-purity (> 99.995 %) tungsten (Toho Kinzoku Co. Ltd.) with a square shape of 7×7 mm^2 and a thickness of 0.3 mm. The samples were mechanically polished and then annealed at 1773 K under vacuum conditions for 2 hours in order to obtain a good quality grain structure for the material analysis releasing rolling stress and enhancing recrystallization.

Helium plasma exposure experiments were carried out using linear plasma device PSI-2 [17]. The tungsten samples were negatively biased at -100 V. Incident helium energy was mono-energetic of 75 eV, since typical ion temperature and plasma potential were a few eV and -25 V, respectively. The incident helium energy was slightly lower than the threshold energy of the sputtering yield and displacement damage. The sample temperature was controlled by a combination of the forced water cooling and the electric heaters, taking into account the heat flux from the plasma. The sample temperature was measured by an infrared (IR) camera and cross-checked with a thermocouple which is installed under the sample. Three identical samples were exposed to helium plasma under each of the following conditions to implement multiple material analyses:

- Temperatures: 473, 773, 1073, 1573 K
- Fluxs: 2.5×10^{20} (low flux), 2.5×10^{22} He/m^{2}s (high flux)
- Fluences: 3.0×10^{23} (low fluence), 1.0×10^{26} He/m^2 (high fluence)

Development of the surface nano structure due to the helium plasma exposure was observed using several surface analysis methods: such as scanning electron microscopy (SEM), transmission electron microscopy (TEM) and electron backscattered diffraction

pattern analysis (EBSD). Focused ion beam (FIB) method was employed to make cross-sectional TEM samples for the depth profile observation of the damage structure and surface morphology.

3. Helium effect on surface morphology

Surface morphology of the helium exposed tungsten is shown in Fig. 1. After exposure to low fluence of 3.0×10^{23} He/m^2, there are almost no differences in damage structure between the low flux and high flux exposure conditions. For both fluxes, slight surface roughness is seen at 473 K, and holes $3 - 15$ nm in diameter are formed at 1073 K. Under He plasma exposure to a fluence of 1.0×10^{26} He/m^2, significant modifications of the surface morphology are observed. A nanoscale undulating surface structure, which has a periodic arrangement, is formed under low temperature conditions below 1073 K. In addition, dark dots about 10 nm in diameter are formed at 473 K, and holes 10 - 30 nm in diameter are formed at 1073 K. A fuzz structure is formed at 1573 K. The fuzz structure is commonly observed in the temperature range between 1000 K and 2000 K as reported in many previous studies [3]. In this study, we focus on the formation of the undulating surface structure in the lower temperature range. Direction and interval of the undulating surface structures strongly depend on each crystal grain and there is a sharp contrasts between adjoining grains, although the structure is uniform within a single crystal grain.

The direction and interval of the undulation in each grain has been measured on the SEM images. Fig. 2 (a) shows the target area used for the analysis. The white contrast at the top center is a dust on the sample which was used to identify the location. The numerals indicate grain identification numbers. The undulating surface structure can be classified into four types, namely, (i) narrow interval, (ii) wide interval, (iii) jagged edge, and (iv) no undulating surface structure, as shown in Fig. 3. The fact that the direction and the interval of the undulating surface structures vary depending on the crystal grain suggests that the crystal orientation might be an important factor in the development of the undulating surface structures.

In order to obtain crystal orientation information of each grain, EBSD analysis has been employed. Since a target depth of the EBSD analysis is several 10 nm and it is similar to the helium irradiation affected depth where the crystal structure is strongly disturbed, it is impossible to obtain an EBSD orientation map after plasma exposure and only random noise can be observed at any grain. In order to solve this problem,

the helium irradiation affected layer is peeled by using a grazing-incidence (10°) focused ion beam (FIB) processing. The peeling depth is approximately 50 nm. This depth is sufficiently deeper than the heavily damaged layer and negligibly shallower than a typical size of the crystal grain. Therefore, this pre-treatment allows us to employ the EBSD analysis even after the plasma exposure experiments. The peeling effect of the surface damaged layer is shown in Fig. 4. In the SEM image (a), the whitish rectangular area is the peeling area and the dark fringe area at the top and the left is the non-peeling area. The EBSD orientation map (b), which was obtained from the same area with the SEM image, shows that the EBSD measurement is possible only in the peeling area.

In the EBSD orientation map (Fig. 2 (b)), the crystal orientation in the normal direction to the surface is expressed by color map (Fig. 2 (c)), and also <100> directions are shown by arrows. The random noise pattern which extends downward from the marker dust is a shadow of the dust because the incident electron beam enters from top with a shallow angle (20°) in the EBSD analysis. The grains which have narrow intervals, namely, #12, #13, #18, #20 and #21, show strong correlation with the {110} plane, which is denoted by green color in the EBSD orientation map. When the grain surface is the {110} plane, one of the <100> should be on the surface because tungsten has a cubic crystal system. The undulating surface structure aligns to the <100> direction as shown in Fig. 5 (#18, #20 and #21). When the grain surface gets tilted from the {110} plane, the interval of the undulating surface structures becomes wider, although the structures also align to the <100> direction which intersects with the surface at the shallowest angle (e.g. #17). If two <100> directions intersect with the surface at approximately the same shallow angle, the edge of the structure becomes jagged (#19, #26). The averaged intervals of the undulation are plotted against the surface inclination from the {110} plane in Fig. 6. The symbol color shows surface crystal orientation which is consistent with Fig. 2. The minimum interval is around 30 nm near the {110} plane (green), and it becomes wider when the surface plane is tilted from the {110} plane. The undulating surface structure does not appear near the {100} plane.

4. Cross-Sectional TEM observation

In order to investigate the three-dimensional structure of the undulation, cross-sectional observation has been carried out using a TEM. The cross-sectional TEM samples have been fabricated by the FIB material processing. In the FIB material processing, physical

sputtering with a very fine ($15 - 150$ nm in diameter) 40 keV Ga ion beam has been employed to excavate a thin samples (approximately area of 15×2 μm^2 and 5 μm in depth) from a surface of the helium irradiated bulk tungsten. And then, the sample has been reduced the thickness using the very fine Ga ion beam until it can be observed by TEM ($\sim$ 50 nm). Fig. 7 shows typical cross-sectional TEM images of the undulating surface structures in (a) narrow and (b) wide interval grain. The profile of the undulating surface structures shows sawtooth shape, that is, one side is steep and the other side has a relatively gentle slope. The height and angle of the steep side slopes (edge) are $\sim$ 8 nm and 50° independently of the interval. He bubbles with a diameter of $1 - 3$ nm are mainly observed in the depth range of 20 nm from the surface. The large flattened bubble which is beyond 10 nm in diameter is formed immediately below the surface, and it becomes a hole structure bursting through the surface. This is the cross-sectional structure of the holes which are observed as dark dots in the SEM images. The most probable mechanism of the large flattened bubble formation is growth and coalescence of the small bubbles which are formed within the narrow range.

The above mentioned surface modifications imply that the significant migration of atoms despite the low energy helium irradiation below the threshold energy of displacement damage ($E_{\mathrm{d}} > 35$ eV [18], displacement damage cannot be caused by low energy helium below 420 eV), and the low temperature condition in which the thermal migration of vacancy cannot be expected ($E_{\mathrm{eff}}^{\mathrm{M}} = 1.8$ eV [19], vacancy migrates significantly around 800 K and above).

Enlarged TEM images, which were taken under (a) the under-focus bright-field condition to emphasize helium bubble image and (b) the phase-contrast condition, are shown in Fig. 8. Bubbles are densely formed within 20 nm depth from the surface, and they can be observed sparsely beyond 50 nm depth. This depth profile of the bubble formation is similar to the helium plasma exposure at the first-wall position in LHD [20]. One of the largest differences between LHD and PSI-2 in the exposure conditions is energy distribution of the incident helium particles. Because the LHD is a confinement device, there are high-energy charge-exchange components which originate from the high-temperature core plasma, and the energy distribution of the incident particles is a rather broad distribution ($1 - 2000$ eV). In PSI-2, on the other hand, the incident energy is mono-energetic of 75 eV. Despite the large difference in the energy distribution which should has an impact on the damage formation depth, the depth distribution of the helium bubble is similar in both experiments. This fact implies that the radiation damage has small impact on the bubble formation.

The lattice-fringe image with the phase-contrast using on-axis beam and 110 diffracted beam (Fig. 8 (b), (c)) shows that the atomic arrangement is significantly perturbed in the surface layer until $7-10$ nm depth. In contrast, the atomic arrangement remains intact in the deep region, as shown in Fig. 8 (d). The lattice-fringe image indicates the lattice spacing of the $\{110\}$ plane, $d_{110} = a/\sqrt{2} \approx 0.22$ nm. These observations show that there is a significant displacement of atoms in the surface layer despite the TRIM-code prediction that no displacement damage occurs with 75 eV helium particles [21]. The depth of the heavily damaged surface layer corresponds to the range of helium particle implantation. A theoretical study shows a possibility of the damage formation (helium bubble and dislocation loop) due to the helium agglomerations at interstices even if there are no pre-induced vacancies [22]. One explanation for the formation of the heavily damaged surface layer should be due to the implanted helium particles.

5. Discussion

The formation mechanism of the undulating surface structure is not known, although it is obvious that the crystal orientation is the key factor. Similar surface structures, which can be observed under high temperature ($1500-1700$ K) and high fluence ($\sim 10^{26}$ He/m^2) conditions, were reported from NAGDIS-I [23] and Pilot-PSI [24]. Dense step structures are observed in the same temperature range in PISCES-A [25]. These surface structures also have variations among grains, and it is reasonable to expect that the crystal orientation has an impact on the surface modifications in the wide temperature range. There are few possibilities to explain the formation mechanism by the analogy with other studies, e.g., crystal orientation dependence of slip [23], sputtering [26] and combined effect of the sputtering and surface diffusion [27, 28]. However, since the undulating surface structure frequently have a jagged edge, the slipping effect is considered unlikely. Regarding the sputtering effects, since the incident helium energy is below the threshold energy of the sputtering yield and the incident angle is normal to the surface in the experiments, it may be irrelevant to apply the model. Furthermore, the fluence dependence at 1073 K (Fig. 1) shows that the undulating surface structure is developed after the hole formation. Therefore, the surface layer is already heavily damaged by helium irradiation before developing the undulating surface structure. A puzzling fact is why original crystal orientation has impact on the surface modifications despite the fact that the surface layer is significantly perturbed by helium irradiation

and it is supposed to be almost losing the information of the original crystal orientation.

6. Conclusion

In the present work, an impact of the crystal orientation on the surface morphology of the helium plasma exposed tungsten has been investigated in the temperature range between 273 K and 1073 K in consideration for the first-wall temperature of the fusion reactor. Surface analyses using the electron microscopy have indicated that a nanoscale undulating surface structure having a periodic arrangement is formed under the temperature below 1073 K, in contrast to the fuzz nanostructure formation in a higher temperature range. The nanoscale undulating surface structure align with the <100> direction, and its interval is the narrowest at the crystal orientation of {110} surface. The interval becomes wider as the crystal grain surface is tilting away from the {110} surface, and the undulating surface structure is not formed near the {100} surface. The height of undulations is $\sim$ 8 nm independently of the interval of the undulations, and it corresponds to the depth of the heavily damaged layer with helium plasma.

Considering tungsten usage in the first-wall of the fusion reactor, it is important whether the undulating surface structure has substantial effects on the surface erosion or not. This calls for further investigations to elucidate the formation mechanism of the undulating surface structure and its effect on the surface erosion.

Acknowledgments

The authors are grateful to the staff of the PSI-2 team for their experimental support and to Mr. D. Nagata for preparing the TEM samples. This work is supported by the IEA Technology Collaboration Programme on the Development and Research on Plasma Wall Interaction Facilities for Fusion Reactors (PWI TCP), and NIFS15ULPP032.

References

[1] G. Pintsuk, "Tungsten as a plasma-facing material", Reference Module in Comprehensive Nuclear Materials, Vol. 4, pp. 551-581 (2012). http://doi.org/10.1016/B978-0-08-056033-5.00118-X

[2] H. Iwakiri, K. Yasunaga, K. Morishita and N. Yoshida, "Microstructure evolution in tungsten during low-energy helium ion irradiation", Journal of Nuclear Materials 283 PART II (2000) 1134-1138. http://doi.org/10.1016/S0022-3115(00)00289-0

[3] S. Kajita, W. Sakaguchi, N. Ohno, N. Yoshida and T. Saeki, "Formation process of tungsten nanostructure by the exposure to helium plasma under fusion relevant plasma conditions", Nuclear Fusion 49 (2009) 095005. http://doi.org/10.1088/0029-5515/49/9/095005

[4] G. De Temmerman, K. Bystrov, J.J. Zielinski, M. Balden, G. Matern, C. Arnas and L. Marot, "Nanostructuring of molybdenum and tungsten surfaces by low-energy helium ions", Journal of Vacuum Science & Technology A 30 (2012) 041306. http://doi.org/10.1116/1.4731196

[5] S. Takamura and Y. Uesugi, "Experimental identification for physical mechanism of fiber-form nanostructure growth on metal surfaces with helium plasma irradiation", Applied Surface Science 356 (2015) 888-897. http://doi.org/10.1016/j.apsusc.2015.08.112

[6] H. Iwakiri, K. Morishita and N. Yoshida, "Effects of helium bombardment on the deuterium behavior in tungsten", Journal of Nuclear Materials 307-311 (2002) 135-138.

[7] V.K. Alimov, W.M. Shu, J. Roth, K. Sugiyama, S. Lindig, M. Balden, K. Isobe and T. Yamanishi, "Surface morphology and deuterium retention in tungsten exposed to low-energy, high flux pure and helium-seeded deuterium plasmas", Physica Scripta T138 (2009) 014048. http://doi.org/10.1088/0031-8949/2009/T138/014048

[8] P.M. Anderson, C.B. Baxi, E.E. Reis, J.P. Smith and P. D. Smith, "Development, installation, and initial operation of DIII-D graphite armor tiles", Fusion Engineering and Design 9 (1989) 3-8. http://doi.org/10.1016/S0920-3796(89)80002-X

[9] H. Horiike, T. Ando, T. Kushima, M. Matsukawa, Y. Neyatani, H. Ninomiya and M. Yamamoto, "Design and development of JT-60 upgrade - Vacuum vessel and first wall", Fusion Engineering and Design 16 (1991) 285-292. http://doi.org/10.1016/0920-3796(91)90199-Z

[10] N. Inoue, A. Komori, H. Hayashi, H. Yonezu, M. Iima, R. Sakamoto, Y. Kubota, A. Sagara, K. Akaishi, N. Noda, N. Ohyabu and O. Motojima, "Design and construction of the LHD plasma vacuum vessel". Fusion Engineering and Design 41 (1998) 331-336.

[11] S. Benhard, J. Boscary, H. Greuner, P. Grigull, J. Kisslinger, C. Li, B. Mendelevitch, T. Pirsch, N. Rust, S. Schweizer, A. Vorkoṗer, M. Weißgerber, "Manufacturing of the Wendelstein 7-X divertor and wall protection", Fusion Engineering and Design 75-79 (2005) 463-468. http://doi.org/10.1016/j.fusengdes.2005.06.102

[12] Y. Someya, K. Tobita, H. Utoh, S. Tokunaga, K. Hoshino, N. Asakura, M. Nakamura, Y. Sakamoto, "Design study of blanket structure based on a water-cooled solid breeder for DEMO", Fusion Engineering and Design 98-99 (2015) 1872-1875. http://doi.org/10.1016/j.fusengdes.2015.05.042

[13] P. Pereslavtsev, C. Bachmann and U. Fischer, "Neutronic analyses of design issues affecting the tritium breeding performance in different DEMO blanket concepts", Fusion Engineering and Design (2015), In Press. http://doi.org/10.1016/j.fusengdes.2015.12.053

[14] E. Lucon, P. Benoit, P. Jacquet, E. Diegele, R. Lässer, A. Alamo, R. Coppola, F. Gillemot, P. Jung, A. Lind, S. Messoloras, P. Novosad, R. Lindau, D. Preininger, M. Klimiankou, C. Petersen, M. Rieth, E. Materna-Morris, H.-C. Schneider, J.-W. Rensman, B. van der Schaaf, B.K. Singh, P. Spaetig "The European effort towards the development of a demo structural material: Irradiation behaviour of the European reference RAFM steel EUROFER", Fusion Engineering and Design 81 (2006) 917-923. http://doi.org/10.1016/j.fusengdes.2005.08.044

[15] D.L. Smith, H.M. Chung, B.A. Loomis, H. Matsui, S. Votinov, W. Van Witzenburg, "Development of Vanadium-Base Alloys for Fusion First-Wall Blanket Applications", Fusion Engineering and Design 29 (1995) 399-410. http://doi.org/10.1016/0920-3796(95)80046-Z

[16] E. Bernard, R. Sakamoto, N. Yoshida and H. Yamada, "Temperature impact on W surface exposed to He plasma in LHD and its consequences for the material properties", Journal of Nuclear Materials 463 (2015) 316-319. http://doi.org/10.1016/j.jnucmat.2014.11.041

[17] A. Kreter, C. Brandt, A. Huber, S. Kraus, S. Möeller, M. Reinhart, B. Schweer, G. Sergienko and B. Unterberg, "Linear Plasma Device PSI-2 for Plasma-Material Interaction Studies", Fusion Science and Technology 68 (2015) 8-14. http://doi.org/10.13182/FST14-906

[18] P.G. Lucasson, and R.M. Walker, "Production and recovery of electron-induced radiation damage in a number of metals", Physical Review 127 (1962) 485-500. http://doi.org/10.1103/PhysRev.127.485

[19] K.-D. Rasch, R.W. Siegel and H. Schltz, "Quenching and Recovery Experiments on Tungsten", Journal of Nuclear Materials 69-70 (1978) 622-624. http://doi.org/10.1016/0022-3115(78)90295-7

[20] M. Thompson, R. Sakamoto, E. Bernard, N. Kirby, P. Kluth, D. Riley and C. Corr, "GISAXS modelling of helium-induced nano-bubble formation in tungsten and comparison with TEM", Journal of Nuclear Materials 473 (2016) 6-12. http://doi.org/10.1016/j.jnucmat.2016.01.038

[21] J.F. Ziegler, J. Biersack and U. Littmark, "The stopping and range of ions in solids", (1985, Pergamon Press)

[22] A.M. Ito, A. Takayama, Y. Oda,T. Tamura, R. Kobayashi, T. Hattori, S. Ogata, N. Ohno, S. Kajita, M. Yajima, Y. Noiri, Y. Yoshimoto, S. Saito, S. Takamura, T. Murashima, M. Miyamoto, H. Nakamura, "Hybrid simulation research on formation mechanism of tungsten nanostructure induced by helium plasma irradiation", Journal of Nuclear Materials 463 (2015) 109-115. http://doi.org/10.1016/j.jnucmat.2015.01.018

[23] N. Ohno, Y. Hirahata, M. Yamagiwa, S. Kajita, M. Takagi, N. Yoshida, R. Yoshihara, T. Tokunaga and M. Tokitani, "Influence of crystal orientation on damages of tungsten exposed to helium plasma", Journal of Nuclear Materials 438 (2013) S879-S882. http://doi.org/10.1016/j.jnucmat.2013.01.190

[24] O. El-Atwani, S. Gonderman, M. Efe, G. De Temmerman, T. Morgan, K. Bystrov, D. Klenosky, T. Qiu and J.P. Allain, "Ultrafine tungsten as a plasma-facing component in fusion devices: Effect of high flux, high fluence low energy helium irradiation", Nuclear Fusion 54 (2014) 083013. http://doi.org/10.1088/0029-5515/54/8/083013

[25] M. Miyamoto, S. Mikami, H. Nagashima, N. Iijima, D. Nishijima, R.P. Doerner, N. Yoshida, H. Watanabe, Y. Ueda and A. Sagara, "Systematic investigation of the formation behavior of helium bubbles in tungsten", Journal of Nuclear Materials 463 (2015) 333-336. http://doi.org/10.1016/j.jnucmat.2014.10.098

[26] R. Smith, "Ripple structures on ion bombarded surfaces arising from the sputter yield dependence on incidence angle", Nuclear Instruments & Methods in Physics Research B 352 (2015) 213-216. http://doi.org/10.1016/j.nimb.2014.11.104

[27] U. Valbusa, C. Boragno and F.B. de Mongeot, "Nanostructuring surfaces by ion sputtering", Journal of Physics: Condensed Matter 14 (2002) 8153-8175. http://doi.org/10.1088/0953-8984/14/35/301

[28] E. Chason and M.J. Aziz, "Spontaneous formation of patterns on sputtered surfaces", Scripta Materialia 49 (2003) 953-959. http://doi.org/10.1016/S1359-6462(03)00474-3

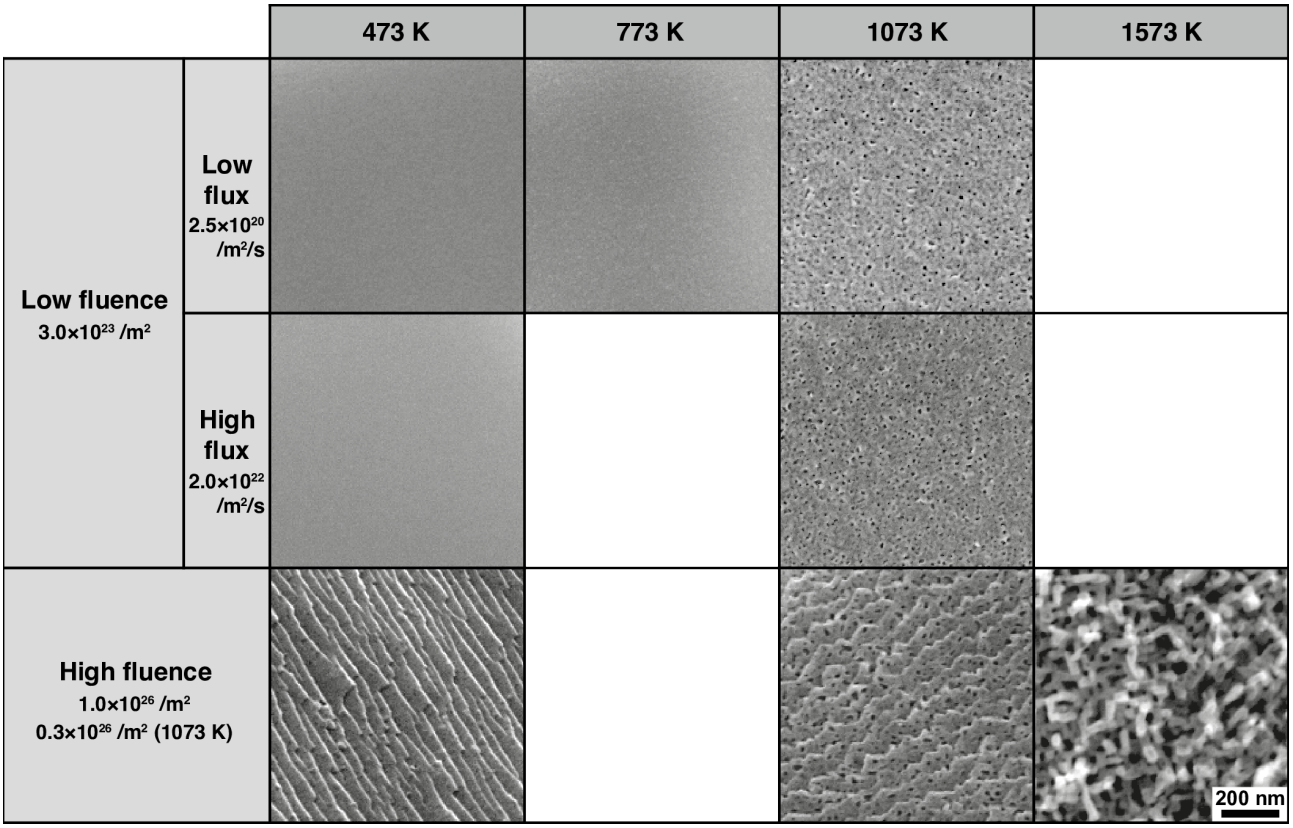

Figure 1. Typical SEM images of tungsten samples irradiated in PSI-2 to a fluence of 3.0×10^{23} (low fluence) and $0.3 - 1.0 \times 10^{26}$ He/m^{2}s (high fluence) at 473, 773, 1073 and 1573 K. Blank spaces mean that the experiments had not been carried out under those conditions.

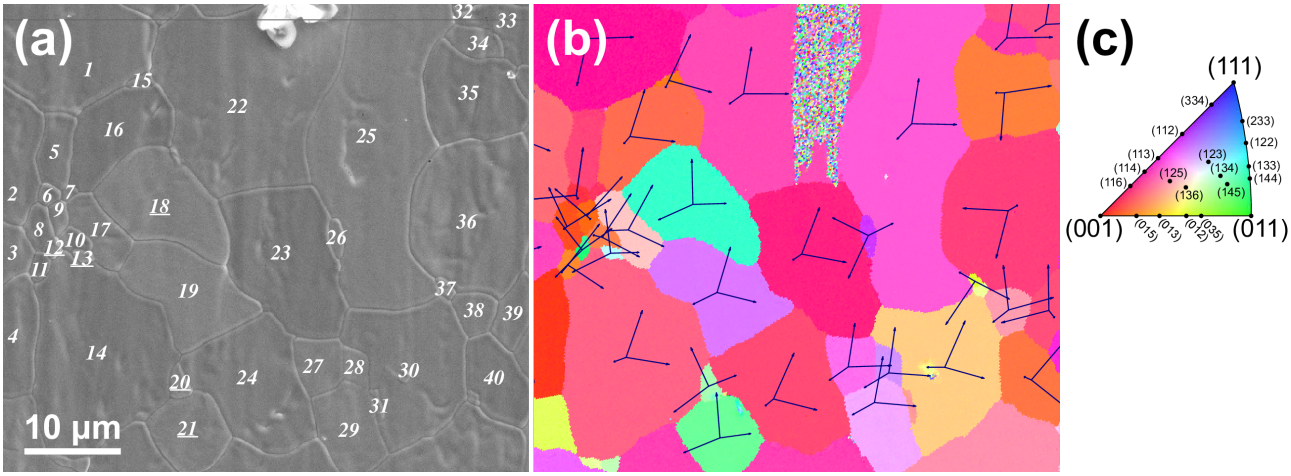

Figure 2. Target area of the comparison study between (a) the surface morphology by SEM and (b) the crystal orientation map by EBSD. Surface crystal orientations are shown by the color map (c). A set of three arrows on each grain indicates projected <100> directions on the grain surface. The helium plasma exposure flux, fluence and sample temperature are 2.5×10^{22} He/m^{2}s, 1.0×10^{26} He/m^2 and 473 K, respectively.

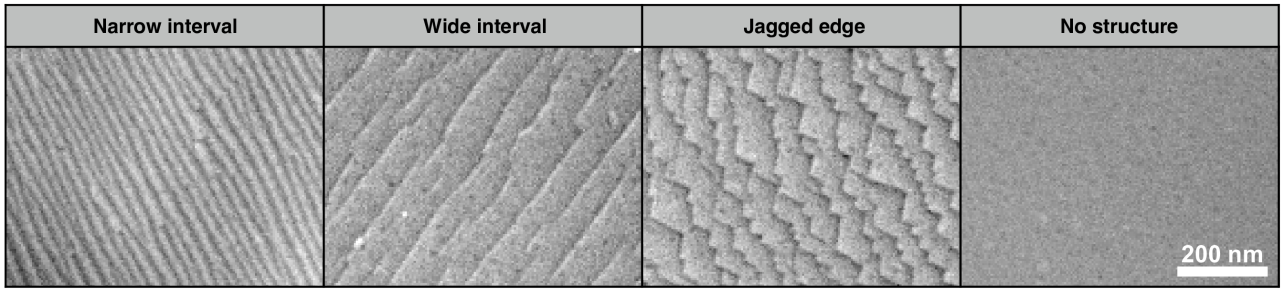

Figure 3. Typical four types of morphology on the helium plasma exposed tungsten surface. The helium plasma exposure flux, fluence and sample temperature are 2.5×10^{22} He/m^{2}s, 1.0×10^{26} He/m^2 and 473 K, respectively.

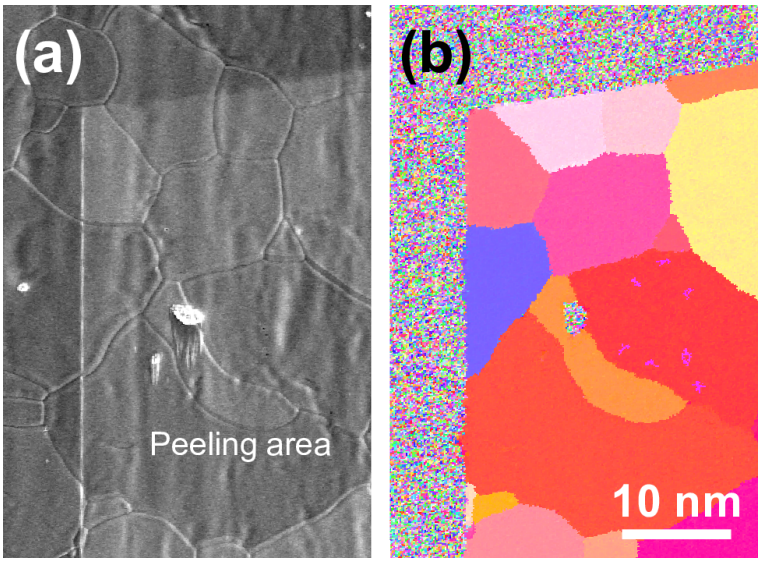

Figure 4. Effect of surface peeling with the FIB on the EBSD analysis. After removing the surface layer of $\sim$ 50 nm damaged during the helium plasma irradiation, EBSD analysis can be carried out. (a) SEM image and (b) EBSD orientation map, at a boundary between peeling area and untreated area.

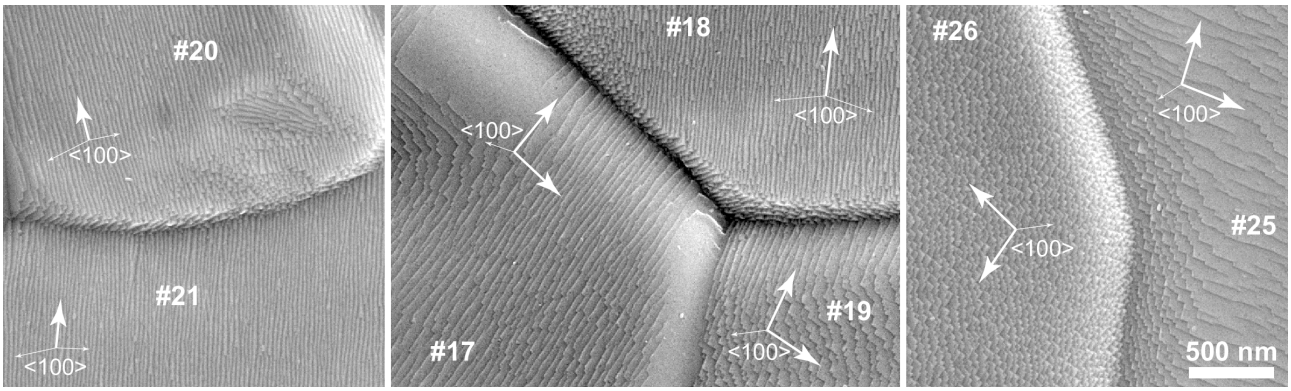

Figure 5. Enlarged SEM image of the helium exposed tungsten up to 1.0×10^{26} He/m^2 with flux of 2.5×10^{22} He/m^{2}s at 473 K, and projected <100> directions on the grain surface. The grain numbers, which are defined in Fig. 2, are also shown.

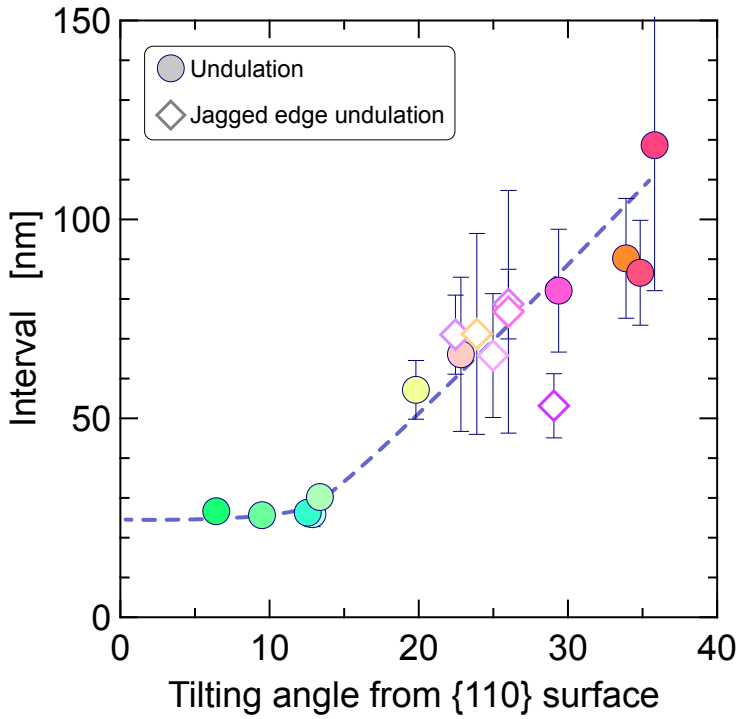

Figure 6. Variation of the averaged interval of undulations with the grain surface orientation based on the tilting angle from the {110} surface. The symbol color shows crystal orientation which is consistent with the EBSD map in Fig. 2.

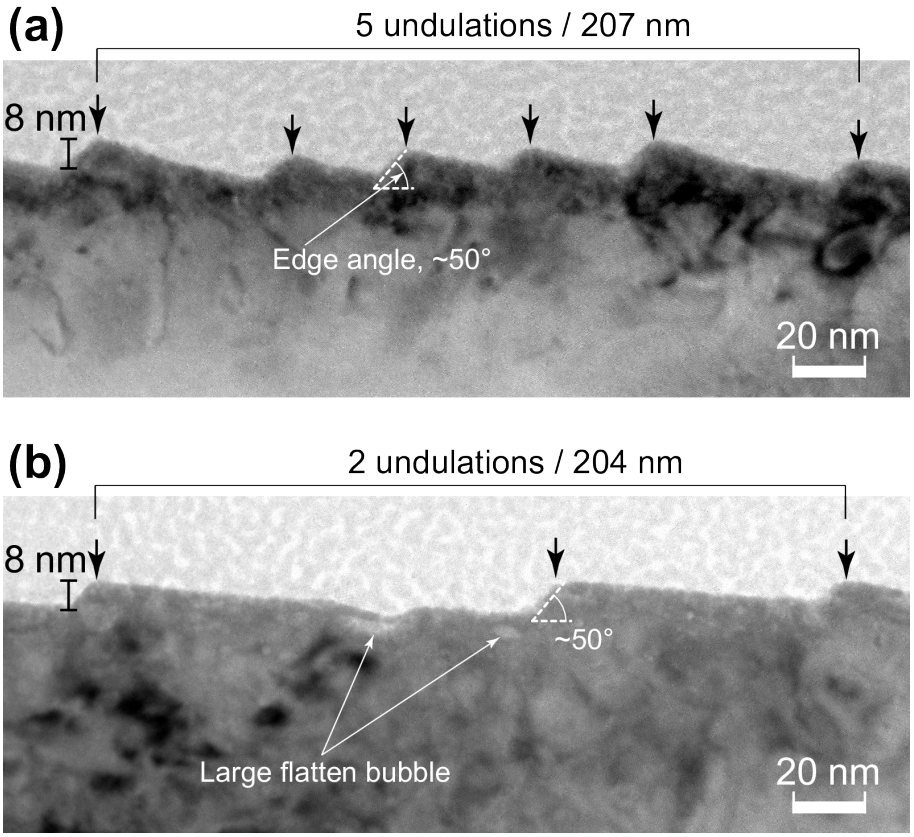

Figure 7. Cross-sectional TEM observation of the undulating surface structures, which have (a) narrow and (b) wide interval. The helium plasma exposure flux, fluence and sample temperature are 2.5×10^{22} He/m^{2}s, 1.0×10^{26} He/m^2 and 473 K, respectively.

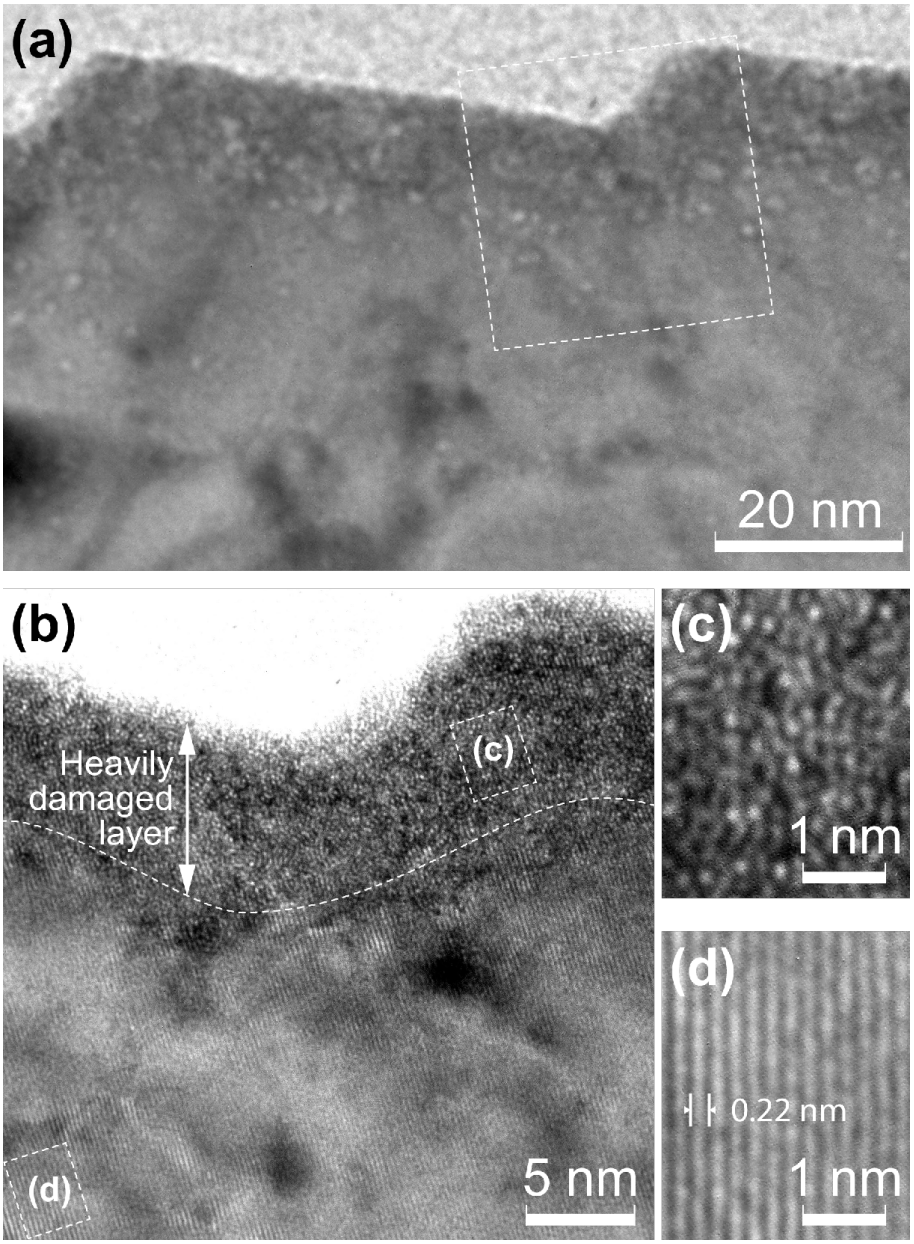

Figure 8. Enlarged cross-sectional TEM image of the undulating surface structures of the helium plasma exposed tungsten up to 1.0×10^{26} He/m^2 with flux of 2.5×10^{22} He/m^{2}s at 473 K under (a) the under-focus bright-field condition, and (b) the phase-contrast condition. The enlarged lattice-fringe images imply heavy damage at the surface layer (c), although the atomic arrangement remains intact in the deep region (d).